Spin dynamics in weakly and strongly interacting NiO nanoparticles

2006 J. Phys.: Condens. Matter 18 11203

(http://iopscience.iop.org/0953-8984/18/49/013)

INSTITUTE OF PHYSICS PUBLISHING JOURNAL OF PHYSICS: CONDENSED MATTER

J. Phys.: Condens. Matter **18** (2006) 11203–11216 doi:10.1088/0953-8984/18/49/013

Spin dynamics in weakly and strongly interacting NiO nanoparticles

C R H Bahl[1,2], K Lefmann[1], L Theil Kuhn[1], N B Christensen[1,3], H Vázquez[1,4] and S Mørup[2]

[1] Materials Research Department, Building 227, Risø National Laboratory, DK-4000 Roskilde, Denmark
[2] Department of Physics, Building 307, Technical University of Denmark, DK-2800 Kongens Lyngby, Denmark
[3] Laboratory for Neutron Scattering, Paul Scherrer Institute, CH-5232 Villigen, Switzerland

E-mail: christian.bahl@risoe.dk

Received 28 June 2006, in final form 3 October 2006
Published 22 November 2006
Online at stacks.iop.org/JPhysCM/18/11203

Abstract

The spin dynamics of plate-shaped nanoparticles of NiO has been studied by inelastic neutron scattering and Mössbauer spectroscopy. A value of the in-plane anisotropy energy constant significantly larger than the bulk value has been measured. The temperature and field dependence of the energy of the antiferromagnetic resonance mode associated with this in-plane anisotropy has been studied. Both Mössbauer spectroscopy and neutron scattering data show that the magnetic fluctuations are strongly affected by the strength of interparticle interactions.

(Some figures in this article are in colour only in the electronic version)

1. Introduction

The spin dynamics of antiferromagnetic nanoparticles differs from that of the corresponding bulk materials. Antiferromagnetic nanoparticles will exhibit superparamagnetism at finite temperatures. This is a thermally activated coherent flipping of the magnetization between the magnetically easy axes. Also, the spin wave spectrum will be quantized, due to the finite size of the particles. The lowest-energy excitation is a spin wave with zero wavevector ($\mathbf{q} = 0$), measured from an antiferromagnetic Bragg reflection. Such spin waves are coherent oscillations of the spins about the ordered moment direction, known as uniform magnetic excitations, and these are the predominant excitations in nanoparticles [1]. In the NiO nanoparticles presented here, there is a large gap, estimated to be ∼10–20 meV, to

[4] Present address: Departamento de Física Teórica de la Materia Condensada, Universidad Autónoma de Madrid, E-28049 Madrid, Spain.

the first $\mathbf{q} \neq 0$ spin wave [2]. Several studies of the spin dynamics in nanoparticles of the antiferromagnet hematite (α-Fe_2O_3) have been conducted [3–5]. Magnetic interactions between the particles have been found by Mössbauer spectroscopy [6, 7] and inelastic neutron scattering [8] to have a strong effect on the spin dynamics. In this paper we present inelastic neutron scattering and Mössbauer spectroscopy studies of weakly and strongly interacting plate-shaped NiO nanoparticles.

1.1. Nickel oxide

NiO has an fcc structure with a bulk unit cell parameter of $a = 4.177$ Å. Below the Néel temperature of 523 K in bulk NiO (460 K in the present nanoparticles [9]) there is a slight contraction of the cubic structure along the [111] direction, known as exchange striction [10]. Early neutron scattering work established that bulk NiO is antiferromagnetic with a $\mathbf{Q}_{\mathrm{AFM}} = \left(\frac{1}{2}\frac{1}{2}\frac{1}{2}\right)$ ordering vector and a confinement of the spins within the (111) plane [11], i.e. a type-II antiferromagnet. Later, an orientation of the spins in the $[11\bar{2}]$ direction within the (111) plane was established [12]. Bulk NiO has a magneto-crystalline anisotropy with a large out-of-plane anisotropy energy constant, K_1, and a much smaller in-plane anisotropy energy constant, K_2 [13]. The anisotropy part of the energy density can be stated macroscopically as in hematite [14]:

$$E = K_1 \cos^2\theta + K_2 \sin^2\theta \sin^2\phi. \tag{1}$$

Here K_i ($i = 1, 2$) are the anisotropy energy constants, θ is the angle between the spins and the [111] direction, and ϕ is the angle between the between the spins and the easy direction within the (111) plane. Anisotropy fields can be defined as $B_{\mathrm{A}i} = \frac{K_i}{M_{\mathrm{S}}}$, where M_{S} is the sublattice magnetization (5.5×10^5 J T^{-1} m^{-3}). As K_1 and K_2 are both positive and $K_1 \gg K_2$, the spins are confined near the (111) plane, making the spin structure essentially two dimensional.

An exchange field can be defined as $B_{\mathrm{E}} = \frac{\mathcal{J}_0 S}{g\,\mu_{\mathrm{B}}}$, where S is the spin of one ion ($S = 1$ in Ni^{2+}) and μ_{B} is the Bohr magneton. $\mathcal{J}_0 = \sum_l z_l J_l$ is the effective exchange constant, where z_l is the number of lth neighbours and J_l is the exchange constant to these. The g-factor is conventionally assumed to be 2, but values of $g = 2.227(2)$ [15] and $g = 2.34(8)$ [16] have been reported for bulk NiO. As will be shown in section 4.4, a value of $g = 2.19(6)$ has been measured in the present nanoparticle sample. In a type-II fcc antiferromagnet, the exchange contributions from the nearest neighbours cancel out [17]. There are six next nearest neighbours with an exchange constant of $J_2 = 221$ K [13] such that $\mathcal{J}_0 = 6J_2$, giving $B_E = 905$ T.

1.2. Uncompensated moments

Long before the advent of 'nanotechnology', Néel proposed that an antiferromagnetic nanoparticle will contain a number of uncompensated spins due the small size of the particle [18]. We define $\xi = \frac{n_2}{n_1}$ as the ratio between the number of spins in the two sublattices. An increase in the number of spins in one sublattice of an antiferromagnetic nanoparticle will change the magnetic properties [19–21] towards those of a ferrimagnet.

A value of $\xi \approx 0.994(1)$ has been obtained by high-field Mössbauer measurements on NiO nanoparticles similar to the particles presented here [22]. It has been suggested that the uncompensated moment may be explained by a random distribution of defects in the particles, by odd numbers of ferromagnetically ordered layers with opposite magnetization directions, or by random occupancy of surface sites [18, 19]. The latter model is in better agreement with the data obtained from Mössbauer spectroscopy than the two others [22]. Magnetization data also suggest that random occupation of surface sites is the main reason for the uncompensated

moment of NiO nanoparticles [19]. The value of $\xi \approx 0.994(1)$ will be assumed in the following, although it will be shown that the exact value is not important for the determined value of the in-plane anisotropy.

1.3. Antiferromagnetic resonance

In the ordered state of an ideal antiferromagnet with the anisotropy energies given by (1) there will be two non-degenerate spin wave branches. The resonance energies, i.e. spin wave energies at the wavevector $\mathbf{q} = 0$, can be approximated at low temperature by [5, 23, 24]

$$\hbar\omega_\alpha \approx g\mu_B\sqrt{2B_E B_{A2}} \tag{2}$$

$$\hbar\omega_\beta \approx g\mu_B\sqrt{2B_E(B_{A2}+B_{A1})} \approx g\mu_B\sqrt{2B_E B_{A1}}. \tag{3}$$

The equations assume $B_E \gg B_{Ai}$ and $B_{A1} \gg B_{A2}$, where $i = 1, 2$ refers to the two anisotropy energy constants.

From neutron scattering measurements on bulk NiO, Hutchings and Samuelsen [13] found a value of the out-of-plane anisotropy energy constant of $K_1 = 4.3(2) \times 10^5$ J m^{-3}, calculated from a resonance mode observed at $\hbar\omega_\beta = 4.5$ meV, in agreement with theoretical and experimental values obtained by others [25–27]. According to [13], the value of the in-plane anisotropy energy constant in bulk NiO is $K_2 = 2.3(1.9) \times 10^4$ J m^{-3}. However, care must be taken when measuring the in-plane anisotropy energy in bulk NiO, as lattice strain may lead to an overestimation of the value, and domain walls may lead to an underestimate of this [28]. Measurements from a strain and domain wall free sample of bulk NiO gave a value of $K_2 = 30$ J m^{-3} [28, 29], i.e. three orders of magnitude less than the value cited in [13].

Far infrared measurements involving two NiO nanoparticle samples with particle sizes of 43.5 and 5.7 nm were presented in [30]. A resonance energy, $\hbar\omega_\beta$, close to that of bulk NiO was found in both samples. Thus, the out-of-plane anisotropy energy constant, K_1, does not depend essentially on the particle size. Apart from preliminary neutron scattering results obtained at a single temperature in zero applied field [31, 32], no study of the in-plane anisotropy and associated resonance mode in nanoparticles of NiO has previously been reported.

This paper reports on a study of the spin dynamics in plate-shaped nanoparticles of NiO by inelastic neutron scattering and Mössbauer spectroscopy. The temperature and field dependence of the ω_α resonance frequency is measured. Nanoparticles of NiO will be shown to have a larger value of K_2 than bulk NiO.

2. Experimental details

Nickel oxide nanoparticles were prepared by heating chemically precipitated $Ni(OH)_2$ in air at 300 °C for 3 h, as described previously [22, 33]. This sample will be referred to as the as-prepared sample. A second sample with reduced interparticle interactions was prepared by separating the particles in the as-prepared sample by low-energy ball milling and subsequently suspending them in water and coating them with a layer of phosphate [33]. These treatments have been shown to result in a significant reduction of the interaction between NiO nanoparticles [33, 34]. This sample will be referred to as the coated sample. Each sample was prepared with a mass of about 5 g, sufficient to perform inelastic neutron scattering and x-ray diffraction.

Samples for Mössbauer spectroscopy were prepared by the same method, but starting with $Ni(OH)_2$ that was doped with about 0.5 at.% ^{57}Fe relative to Ni [22, 33, 34]. These samples were prepared at a smaller scale than the undoped samples, each sample having a mass of about 50 mg.

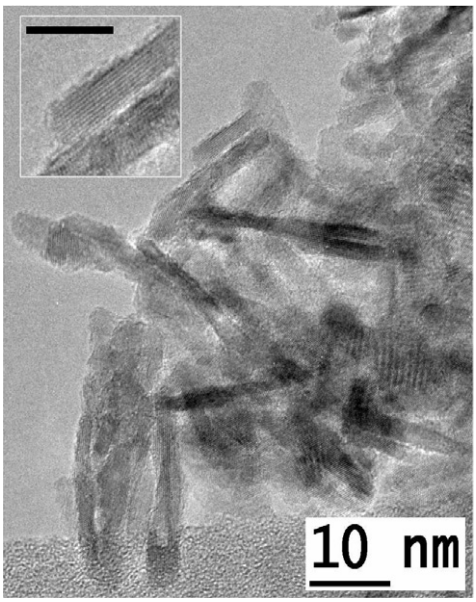

Figure 1. TEM image of an agglomerate of NiO particles in the as-prepared sample. The inset shows a magnified image of one of the plate-shaped particles viewed edge-on. The scale bar in the inset is 5 nm. The visible planes are the (111) planes, which are seen to be parallel to the plate face.

High-resolution transmission electron microscopy (TEM) was performed on the undoped samples using a JEM 3000F FEG microscope equipped with a 16 Mpix CCD camera. X-ray diffraction (XRD) on the undoped samples has been carried out using Cu Kα radiation in a Philips PW 1820 diffractometer.

Mössbauer spectra were obtained in the temperature range from 6 to 295 K using a source of ^{57}Co in a rhodium matrix. Above 80 K the samples were cooled in a temperature-controlled liquid nitrogen cryostat. At temperatures below 80 K the samples were cooled in a closed-cycle helium refrigerator, and below 20 K the samples were cooled in a liquid helium cryostat.

Inelastic neutron scattering was conducted at a range of temperatures on the as-prepared sample using the TAS7 triple-axis spectrometer at Risø National Laboratory and on the coated sample using the RITA-II triple-axis spectrometer at the Paul Scherrer Institute in Villigen, Switzerland. On TAS7 the signal was detected using a single analyser and detector at final neutron energies of $E_f = 5.0$ meV. The RITA-II spectrometer is equipped with a multiblade analyser and position-sensitive detector [35]. This multiblade analyser was used in the newly implemented imaging mode [35, 36] also at a final neutron energy of $E_f = 5.0$ meV. At both spectrometers, a Be filter was used to remove high-energy neutrons. Both temperature series were performed in the range 10–330 K using a closed-cycle helium refrigerator. At RITA-II, a field series on the coated sample in the range 0–13.5 T at 200 K was obtained using an Oxford 15 T magnet.

3. Results

3.1. Size and morphology

The size and morphology of the particles have been investigated by transmission electron microscopy (TEM); see figure 1. In both samples the particles were found in large, loosely

packed agglomerates. The interaction between nanoparticles is difficult to observe by TEM. A layer without visible lattice fringes, presumably due to adsorption of water and organic molecules from atmospheric air, is found to cover the surfaces of the particles in both samples. The phosphate coating of the coated sample may not be distinguished from the layer due to adsorption. The subtlety of the interaction between NiO nanoparticles is demonstrated in [34], where it is shown that long-term exposure to a humid atmosphere can significantly reduce the interparticle interaction.

The particles were observed to be disc shaped, with a thickness of 2.3 ± 0.4 nm in both samples and a diameter of 13 ± 3 nm in the as-prepared sample and 12 ± 2 nm in the coated sample. The listed uncertainties represent the standard deviation of the size distributions. In addition, it is observed in both samples that the faces of the discs are (111) planes. High-resolution TEM images show that the plate faces are not perfectly plane, but contain steps and kinks [22]. Except for the disc faces, no facets are observed.

The XRD patterns of the as-prepared and coated samples have been fitted using profile refinement in the software package FullProf [37]. Assuming a platelet shape, as described elsewhere [22], an estimated plate thickness of 2.3 nm and a diameter of $\sim$7.5 nm was obtained in both samples. The thicknesses are consistent with those found in TEM, but the diameters are underestimated compared to TEM. As discussed previously [22], this is probably due to particle size distributions giving difficulties in fitting the sharpest part of some of the reflections. Another possibility may be that each individual particle consists of more than one crystallite, but this has not been observed by high-resolution TEM.

Thus the particle size and morphology of the as-prepared and the coated samples are identical within experimental uncertainty. The ^{57}Fe-doped NiO nanoparticles have the same size and morphology as the undoped particles [38]. However, because the particles used for neutron scattering and Mössbauer spectroscopy were not taken from the same batch, there may be small differences, and a direct comparison between, for example anisotropy energies and interaction energies, should be taken with some reservation.

3.2. Mössbauer spectroscopy

Mössbauer spectra of the as-prepared and coated samples are shown in figure 2. The coated sample shows a behaviour typical for non-interacting or weakly interacting superparamagnetic particles [6, 8, 39]. The spectra consist of a superposition of a sextet due to particles with a relaxation time longer than the timescale of Mössbauer spectroscopy ($\sim$ a few nanoseconds) and a singlet due to particles with shorter relaxation time. The relative area of the singlet increases with increasing temperature, because of the temperature dependence of the relaxation time. At 295 K, almost all particles exhibit fast superparamagnetic relaxation. At 20 K a doublet with a small intensity is also visible; this is presumably due to iron atoms that have reacted with the phosphate layer, coating the nanoparticles. At elevated temperatures the area of the doublet is negligible compared to the singlet component, and therefore not observed. The spectra of the as-prepared sample show a quite different behaviour. Below 150 K the spectra consist of sextets and no singlet component is visible. Instead, the lines of the sextet become increasingly broadened with increasing temperature and the average hyperfine field decreases rapidly with increasing temperature. This behaviour is typical for samples of interacting nanoparticles for which the relaxation may be described as fluctuations of the sublattice magnetization around a direction mainly defined by an interaction field rather than fluctuations between two minima in opposite directions [6, 8, 39]. Similar results have been found in previous studies of weakly and strongly interacting nanoparticles of hematite [6, 8], NiO [22, 33, 34] and maghemite (γ-Fe_2O_3) [40].

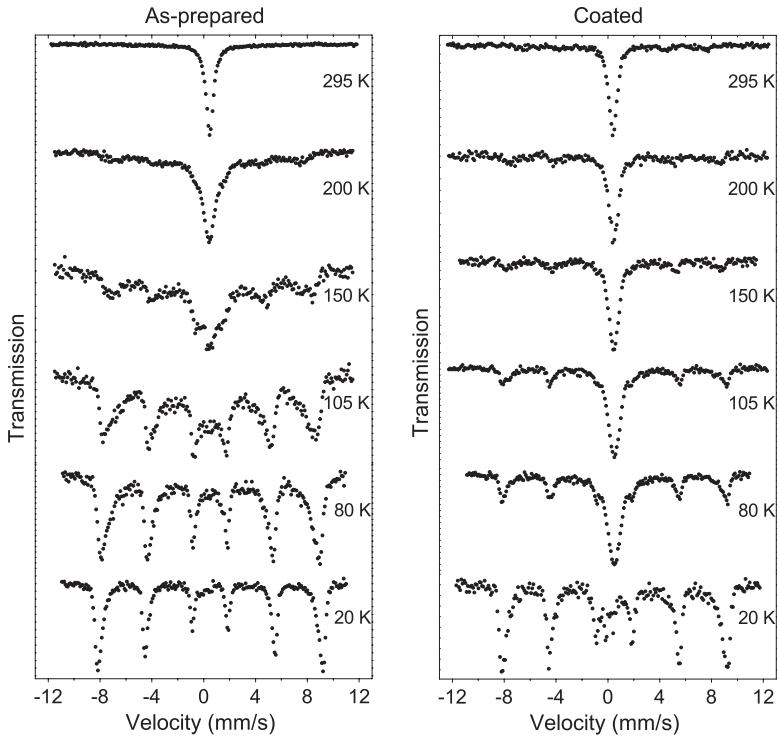

Figure 2. Mössbauer spectra of the ^{57}Fe-doped NiO nanoparticles in the as-prepared and coated samples recorded at temperatures in the range 20–295 K. The low-temperature data are fitted with a distribution of sextets, as discussed in section 4.1.

3.3. Inelastic neutron scattering

Inelastic neutron scattering was performed with the scattering vector, $\boldsymbol{\kappa}$, equal to the antiferromagnetic ordering vector $\mathbf{Q}_{\mathrm{AFM}} = \left(\frac{1}{2}\frac{1}{2}\frac{1}{2}\right)$. As the samples are powders, only the magnitude of the scattering vector is measured and $\kappa = Q_{\mathrm{AFM}} = 1.30$ Å^{-1}. Inelastic scans obtained at Q_{AFM} from the coated sample at 200 K in zero applied field and an applied field of 4 T are shown in figure 3. The inelastic scans reveal a quasielastic central peak and broad shoulders on both sides of this. This type of spectrum is well known from previous studies of hematite nanoparticles [3, 4]. The broad shoulders have been shown to be due to uniform magnetic excitations, and could be modelled with a damped harmonic oscillator model. The exponential relaxation rate of superparamagnetism results in an additional Lorentzian broadening of the quasielastic line shape. The dynamics can be described as [3, 4]

$$I(\varepsilon) = A_0\delta(\varepsilon) + W(\varepsilon)D(\varepsilon) + \frac{A_1}{\pi}D(\varepsilon)\frac{\Gamma}{\varepsilon^2+\Gamma^2} + \frac{A_2}{\pi}D(\varepsilon)\frac{2\gamma\varepsilon_0^2}{(\varepsilon^2-\varepsilon_0^2)^2+4\gamma^2\varepsilon^2} + C \qquad (4)$$

where A_1 is the area of the quasielastic peak and A_2 is the area of the inelastic components. A_0 is the area of the incoherent elastic background, $W(\varepsilon)$ is the contribution from adsorbed water, and C is the incoherent inelastic background. ε_0 is the position of the inelastic peaks on either side of zero, γ is the width of these peaks, and Γ is the width of the quasielastic peak. $D(\varepsilon)$ is the detailed balance factor, due to a difference in the population of the creation and annihilation

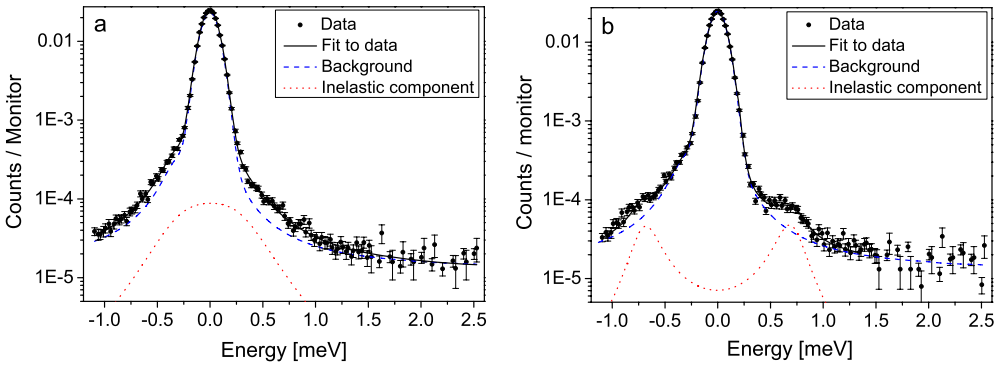

Figure 3. Inelastic neutron scattering data recorded from the coated sample at 200 K. The data points are obtained at the antiferromagnetic reflection and the solid line is a fit to this. The dashed line is a fit to the incoherent background data (not shown) and the dotted line is a plot of the inelastic component convoluted with the resolution function. (a) Data obtained at zero applied field showing a broad inelastic signal. (b) Data obtained with an applied field of 4 T.

states of uniform excitations, it is given at a temperature, T, by[5]

$$D(\varepsilon) = \frac{\varepsilon}{k_B T}\left(\frac{1}{\exp\left(\frac{\varepsilon}{k_B T}\right) - 1} + 1\right) \tag{5}$$

where k_B is Boltzmann's constant. Due to the extremely large surface area of the nanoparticles, water will inevitably be adsorbed during and after preparation. The water scatters neutrons incoherently with increasing mobility as the temperature is increased, resulting in a Lorentzian line shape, $W(\varepsilon)$, with increasing width as the temperature is increased. All the above-mentioned contributions must be convoluted with the resolution function of the spectrometer before fitting can be done. The resolution function has been determined to be the sum of a Gaussian and a much weaker Lorentzian, measured by fitting spectra recorded at low temperature. At each temperature, the background spectrum, including the contribution from adsorbed water, is fitted from scans at scattering vectors in the incoherent background on both sides of Q_{AFM}, i.e. $Q_{incoh} = 1.00$ and 1.60 Å^{-1}. Keeping these fixed, the remaining parameters in (4) are obtained from fits to the spectra at Q_{AFM}.

Parameters obtained from the fits to (4) are given in figures 4 and 5 and will be discussed in the following.

4. Discussion

According to the results of [30], discussed in section 1.3, the value of the out-of-plane anisotropy energy constant in NiO nanoparticles is similar to that found in bulk NiO. Using this value of the anisotropy energy constant and the volume obtained from TEM, an out-of-plane particle anisotropy of $K_1 V/k_B \approx 9000$ K may be estimated. From polarization arguments, the resonance mode associated with the out-of-plane anisotropy is not observable at $\kappa = 1.30$ Å^{-1}, but at the $\left(\frac{3}{2}\frac{1}{2}\frac{1}{2}\right)$ reflection at $\kappa = 2.50$ Å^{-1}. Due to the geometrical constraints of the cold neutron spectrometer employed and the sharp decrease in scattering intensity as the energy

[5] Note that this definition of the detailed balance factor differs from that stated in [3–5] due to a typing error there. The data in these publications were, however, fitted using the correct expression.

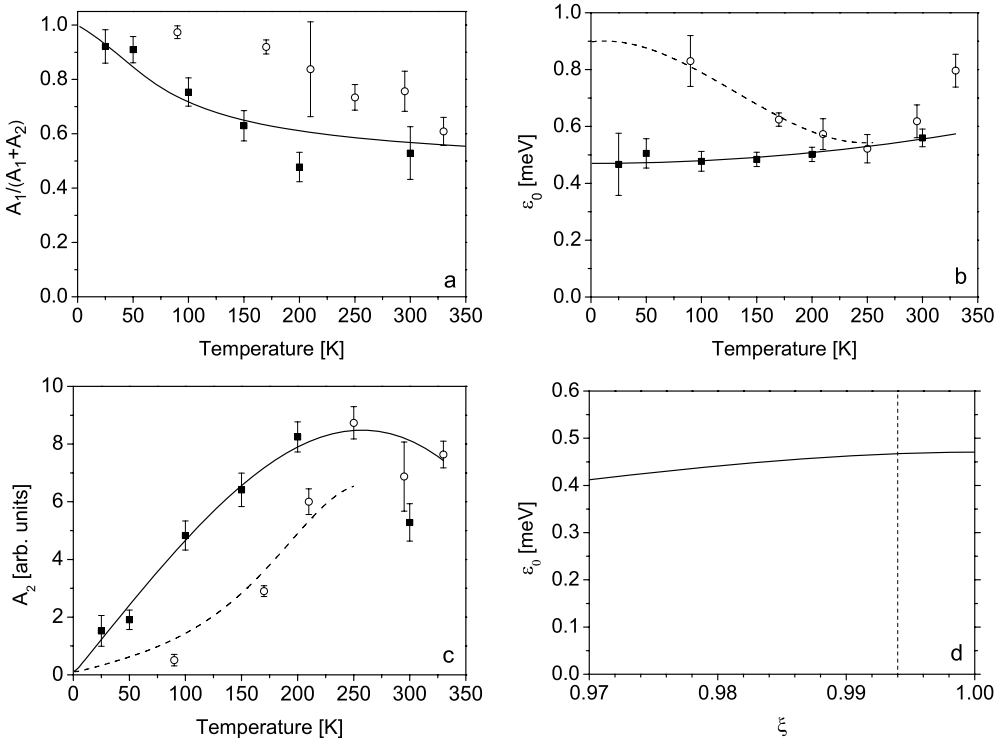

Figure 4. Fits to inelastic neutron scattering data obtained at a range of temperatures in zero applied field. ○ is data from the as-prepared sample and ■ is data from the coated sample. The lines are fits to the data discussed in the text. Full lines are fits to the data from the coated sample and the dashed lines are fits to the data from as-prepared sample. (a) The ratio of the inelastic signal to the total magnetic signal. (b) The position of the inelastic signals. (c) The intensity of the inelastic signal. (d) The resonance energy of the ω_α mode as a function of the ratio between the number of atoms in the two sublattices. The vertical line indicates the value of this ratio measured in [22].

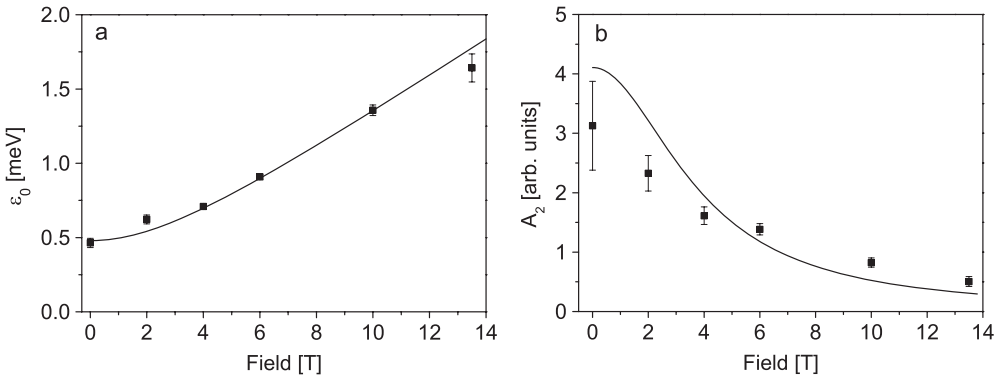

Figure 5. Parameters obtained from fits to inelastic neutron scattering data obtained from the coated sample at 200 K at a range of applied fields. The lines are fits to the data, as discussed in the text. (a) The field dependence of the position of the inelastic signal. (b) The intensity of the inelastic signals.

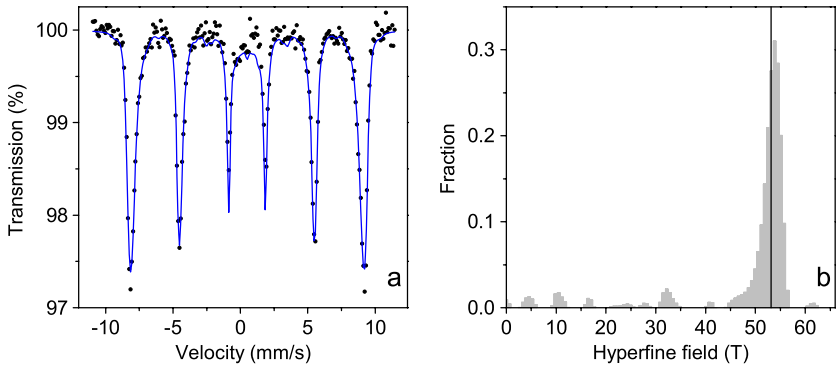

Figure 6. Mössbauer spectrum of the as-prepared sample at 20 K. (a) The spectrum is fitted with a distribution of sextets. The line indicates the sum of the sextets. (b) The distribution of hyperfine fields in the sextet component. The vertical line indicates the median hyperfine field.

transfer increases, measurement of the resonance mode ω_β was not feasible. Thus, in the following we shall assume the same value of K_1 as for bulk NiO.

4.1. Mössbauer spectroscopy data

At the lowest temperatures the Mössbauer spectra of both samples display a magnetically split sextet with a hyperfine field of about 54 T. As the temperature is increased the hyperfine field gradually diminishes. This reduction is due to the influence of collective magnetic excitations and can be described by [41]

$$B_{\mathrm{obs}}(T) \approx B_0(T)\left[1 - \frac{k_{\mathrm{B}}T}{2E_{\mathrm{a}}}\right] \tag{6}$$

where $B_0(T)$ is the hyperfine field in the absence of collective magnetic excitations in the sample at a temperature T, $B_{\mathrm{obs}}(T)$ is the measured hyperfine field and V is the particle volume. In order to take into account the particle size distribution the low-temperature spectra were fitted with a distribution of sextets [42]. Figure 6 shows such a fit and the distribution of hyperfine fields for the as-prepared sample at 20 K. The median of the hyperfine field distribution is indicated by a line. The temperature dependence of the median hyperfine fields, obtained in this way, were fitted with straight lines, as shown in figure 7. From the slopes, median values of E_{a} were calculated. As discussed above, iron that has reacted with phosphate contributes a small doublet component. This doublet component is fitted separately. At 15 K the doublet covers about 6% of the spectral area. The data from the coated sample at 6 K has been omitted as the doublet component due to the phosphate orders to a sextet, making fitting unreliable.

For the anisotropy configuration of NiO, E_{a} is related to the magneto-crystalline anisotropy by [6, 41]

$$\frac{1}{E_{\mathrm{a}}} = \frac{1}{2K_2V + E_{\mathrm{int}}} + \frac{1}{2K_1V + E_{\mathrm{int}}} \tag{7}$$

where E_{int} is related to the interaction energy of the interparticle interactions.

The linear fits to the low-temperature Mössbauer data in figure 7 yield values of $E_{\mathrm{a}}/k_{\mathrm{B}} = 310(30)$ K for the coated sample and $E_{\mathrm{a}}/k_{\mathrm{B}} = 650(50)$ K for the as-prepared sample. Assuming that the bulk value of $K_1V/k_{\mathrm{B}} = 9000$ K and that the coated sample has a

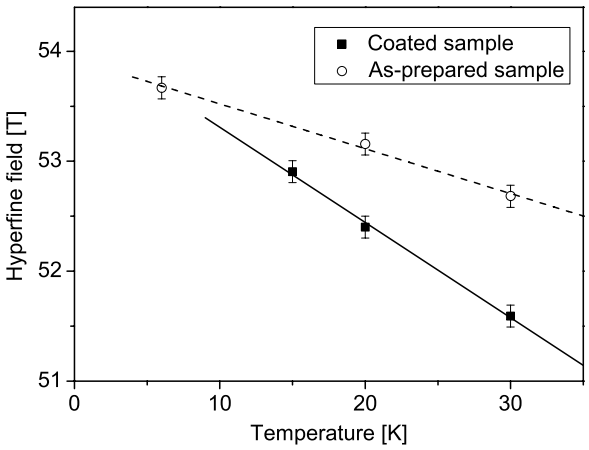

Figure 7. Linear fits to the average hyperfine field splittings measured at low temperatures in the as-prepared and coated samples.

negligible interaction energy, the in-plane anisotropy of the coated sample becomes $K_2V/k_B = 155(15)$ K, equivalent to $K_2 = 8.2(8) \times 10^3$ J m^{-3} or $B_{A2} = 15(2)$ mT. If the as-prepared sample is assumed to have the same in-plane anisotropy, K_2, the interaction energy is calculated from (7) to be $E_{int}/k_B = 360(60)$ K.

4.2. Inelastic neutron scattering data

Due to the nearly cubic nature of the crystal structure, there will be four almost equivalent sets of {111} planes. One of these is the (111) plane, in which the spins are confined uniquely, defined by the exchange striction. The other three are at an angle of ≈70.5° to this. However, the magnetic structure factors of the three $\{\frac{1}{2}\frac{1}{2}\frac{1}{2}\}$ reflections corresponding to the latter three planes are all zero, none of them contributing any scattering intensity.

The scattering intensity of the inelastic signal, $A_2D(\varepsilon)$ at Q_{AFM} with zero spin wavevector, i.e. infinite wavelength, is given by [43]

$$I(\varepsilon, Q_{AFM}) \propto \frac{\mathcal{J}_0\langle S\rangle^2}{\varepsilon_0}\sum_{\alpha}[1-\hat{\kappa}_\alpha^2]\Big[\big(n(\varepsilon)+1\big)\delta(\varepsilon-\varepsilon_0)+n(\varepsilon)\delta(\varepsilon+\varepsilon_0)\Big]. \tag{8}$$

Here $\langle S\rangle$ is the thermal average of the spin, $n(\varepsilon) = (\exp(\frac{\varepsilon}{k_BT}) - 1)^{-1}$ is the Bose factor, and δ is the Dirac delta function. α is a cartesian coordinate and $\hat{\kappa}_\alpha$ is the α component of the unit scattering vector along the spin fluctuation direction. Note that ε_0 is proportional to $\langle S\rangle$, giving the conventional linear dependence of the cross section on $\langle S\rangle$ [44]. Due to the large out-of-plane anisotropy energy, the precession will be strongly elliptical, with the long axis in the (111) plane. This has been confirmed experimentally for hematite, which has a similar anisotropy structure [5]. In this case the cartesian coordinate sum in (8) is approximately $[1-\hat{\kappa}_\beta^2]$, where β is in the direction of the long axis of the ellipse. As β is preferentially in the (111) plane and thus perpendicular to the scattering vector, this factor will give its maximum value, $\hat{\kappa}_\beta^2 \approx 0$.

In the case of superparamagnetism, the dynamics is longitudinal, with the spins flipping between the easy axes. The intensity of the resulting quasielastic signal will contain a cartesian coordinate sum equivalent to the one in (8). This sum simplifies to $[1-\hat{\kappa}_z^2]$, with $\hat{\kappa}_z$ the component of the unit scattering vector along z. Again, there is a maximum scattering intensity as Q_{AFM} is perpendicular to z, giving $\hat{\kappa}_z^2 = 0$.

4.3. Resonance parameters in zero field

4.3.1. Intensity ratio. Figure 4(a) shows the intensity ratio of the quasielastic signal over the total magnetic signal, $A_1/(A_1 + A_2)$, for both samples as a function of temperature. The anisotropy energies may be calculated from the low-temperature data using (8) in [4], which is derived from Boltzmann statistics. The intensity ratio depends only weakly on K_1V/k_B, so this is fixed to the bulk value of 9000 K. Fitting the data at temperatures below 175 K yields a value of $K_2V/k_B = 200(45)$ K, equivalent to $K_2 = 11(2) \times 10^3$ J m^{-3} or an anisotropy field of $B_{A2} = 20(5)$ mT, which is close to the result obtained from Mössbauer spectroscopy. No model for the intensity ratio in the complex situation of interacting particles is available.

4.3.2. Resonance energy. At low temperature the centre position of the inelastic signal in the coated sample is $\varepsilon_0(0) = 0.47(1)$ meV, as seen in figure 4(b). By (2), this gives an anisotropy field of 7.6(3) mT, equivalent to $K_2 = 4.2(2) \times 10^3$ J m^{-3}. This value is significantly less than the values of K_2 obtained by both low-temperature Mössbauer spectroscopy and the area method presented above. There may be several reasons for this underestimate of the in-plane anisotropy. Most likely it is due to an overestimate of the exchange field. As many of the ions are at surface sites with lower numbers of exchange bonds compared to the bulk value, a decrease in the exchange field of 10% may be justified. Also, the value of the exchange constant itself may be overestimated, as a value of $J_2 = 202$ K has been reported for bulk NiO [45]. Lastly, it is well known from previous work on similar nanoparticles that there is a significant amount of spin canting in the particles [22]. This may arise around defects in the structure and at surface sites [46]. The misalignment of the spins due to canting will also reduce the exchange field. Calculating the exchange field required to account for the measured resonance energy while assuming an anisotropy field of 15 mT gives a value of $B_E = 460$ T or about half the bulk value.

The dependence of the resonance energy of mode ω_α on the ratio between the number of spins on the two sublattices, ξ, has been calculated in [24] and plotted in figure 4(d). Here, the out-of-plane anisotropy field is set to 0.73 T, according to [30], and the in-plane anisotropy field is set to 15 mT, as determined by Mössbauer spectroscopy. Previously, the ratio of the number of spins on the two sublattices was measured to be $\xi = 0.994$ [22]. At this value the reduction of resonance energy is negligible, as illustrated in figure 4(d). Thus, no correction of the determined anisotropy energy due to the presence of uncompensated moment is necessary.

4.3.3. Temperature dependence of the resonance energy. As the temperature is increased, the centre position of the inelastic signal is almost constant, increasing slightly at high temperatures. This disagrees with the temperature dependence previously calculated by Boltzmann statistics [4], where the resonance energy was found to decrease with temperature when the system approaches the non-harmonic range of the energy landscape in (1). The observed temperature dependence of the precession energy is empirically approximated by a quadratic expression in temperature, shown as the solid line in figure 4(b).

The centre position of the inelastic signal in the as-prepared sample is found at a higher value than in the coated sample. As the temperature increases, the effect of the interparticle interactions decreases until the resonance energies in the two samples become the same at about 250 K. This temperature corresponds approximately to the interaction energy estimated from Mössbauer spectroscopy. The resonance energy of the as-prepared sample has also empirically been fitted with a polynomial expression.

In both samples the resonance energy seems to increase above 250 K. However, this is presumably because the model used to fit the data (equation (4)) is not valid at high

temperatures. Well below 250 K, the dynamics can be described as a combination of uniform excitations with small amplitude (which give rise to the inelastic peaks) and superparamagnetic relaxation, i.e. reversal of the sublattice magnetization vectors (which gives rise to a broadening of the quasielastic peak) as described by (4). At temperatures of the order of 250 K, the thermal energy becomes comparable to the anisotropy energy, K_2V. Then the two types of magnetic dynamics cannot be separated clearly, because the sublattice magnetization vectors can fluctuate with similar probabilities in all directions in or close to the (111) plane. The transition to this isotropic relaxation regime has been discussed by Würger [47]. For this reason, the data obtained above 250 K are not included in the fits.

4.3.4. Scattering intensity. Using the quadratic expression for the resonance energy determined above, the scattering intensity of the inelastic signal from the coated sample can be calculated by (8) within a proportionality factor. Normalizing this by the detailed balance factor, it may be fitted to the inelastic intensity, A_2, obtained by fitting the data with (4). The reduction in $\langle S \rangle$ with temperature is taken from the data in [9]. The intensity, plotted in figure 4(c), increases linearly up to 200 K, where it flattens out due to the increase in ε_0. For the as-prepared sample the increased energy required to excite the collective magnetic excitations (compared to the coated sample) will result in a reduction in the intensity from the inelastic signal. This suppression of the uniform magnetic excitations due to interactions was also observed in the low-temperature Mössbauer data. Using the empirical fit to the data in figure 4(b), the intensity is again calculated by (8), giving the dashed line plotted in figure 4(c), in qualitative agreement with the measured data.

4.4. Field dependence of resonance parameters

We only measure scattering from particles with the [111] direction along the scattering vector. Thus, all the particles that contribute have identically oriented (111) planes, as the field is applied perpendicular to the scattering vector. There is no component of the field out of the plane, and the strongly elliptical nature of the precessions is not expected to be affected by the field, so the value of the cartesian coordinate sum in (8) is independent of the field and will always be at its maximum value as $\hat{\kappa}_\beta \approx 0$.

At high applied fields the moment of a particle will align with the applied field. The spins will experience the sum of the applied field and the in-plane anisotropy field. Integrating this sum for all orientations of the anisotropy field gives an expression for the resonance energy of

$$\hbar\omega = \sqrt{\varepsilon_0^2 + (g\mu_B B_{\mathrm{appl}})^2}. \tag{9}$$

This expression is valid at zero applied field and at large applied fields. It is not valid in moderate applied fields, where the spin dynamics enters a complex regime in which the anisotropy field acting on all the spins and the applied field acting on the uncompensated spins become similar in size. The energy expression in (9) has been fitted to the field data obtained from the coated sample at 200 K. The fit was performed by omitting the data at 2 and 4 T as the expression is not presumed to be valid here. The fit is shown in figure 5(a). Except at 2 T, the expression fits the data well. The fit gives a value of $\varepsilon_0 = 0.48(3)$ meV and a value of the g-factor of $g = 2.19(6)$. This value of the g-factor is in accordance with the reported observations of non-quenched orbital momentum in NiO [15, 16].

Calculating the scattering intensity of the inelastic signal by (8) as a function of the applied field gives the line in figure 5(b). The calculated intensity is observed to be in qualitative agreement with the measured data except at the lowest applied fields.

5. Conclusion

Inelastic neutron scattering and Mössbauer spectroscopy have been employed to study the spin dynamics in a sample of interacting nanoparticles of NiO and one where the interactions have been removed by phosphate coating. Consistent values of the in-plane anisotropy energy constant in the weakly interacting nanoparticles have been measured by inelastic neutron scattering and Mössbauer spectroscopy, arriving at values more than two orders of magnitude larger than the bulk value. The temperature dependences of the resonance energies measured by neutron scattering could not be fully explained by the present model, so empirical models were employed. Interactions between the particles were observed to significantly increase the resonance energy, reducing the scattering intensity. A model assuming alignment of the particle moments in large applied fields, due to the presence of an uncompensated moment, was used to fit the field dependence of the resonance energy in the weakly interacting particles. The scattering intensities fit well using both the field model and the empirical temperature models for the resonance energy.

Acknowledgments

This project was supported by the Danish Technical Research Council through the Nanomagnetism programme. We thank P-A Lindgård for valuable discussions, L Lilleballe for help with the sample preparation, H K Rasmussen for help with Mössbauer measurements, and Ch Niedermayer and C Kägi for help with the neutron scattering measurements. We gratefully acknowledge the Danish Neutron Scattering Centre (DANSCATT) for financial support for the neutron scattering experiments. This work is based on experiments performed at the Swiss spallation neutron source SINQ and the Paul Scherrer Institute, Villigen, Switzerland. The 15 T magnet used at SINQ was funded by The Swiss National Science Foundation (through both NCCR/MaNEP, and R'EQUIP programs) as well as The Danish Natural Science Research Council and the Carlsberg Foundation. We also thank the EC-TMR-Access to the Large Scale Facilities programme for funding the neutron scattering at the Risø National Laboratory.

References

[1] Mørup S and Hansen B R 2005 *Phys. Rev.* B **72** 024418
[2] Hendriksen P V, Linderoth S and Lindgård P-A 1993 *Phys. Rev.* B **48** 7259
[3] Hansen M F, Bødker F, Mørup S, Lefmann K, Clausen K N and Lindgård P-A 1997 *Phys. Rev. Lett.* **79** 4910
[4] Klausen S N, Lefmann K, Lindgård P-A, Clausen K N, Hansen M F, Bødker F, Mørup S and Telling M 2003 *J. Magn. Magn. Mater.* **266** 68
[5] Klausen S N, Lefmann K, Lindgård P-A, Theil Kuhn L, Bahl C R H, Frandsen C, Mørup S, Roessli B, Cavadini N and Niedermayer C 2004 *Phys. Rev.* B **70** 214411
[6] Hansen M F, Koch C B and Mørup S 2000 *Phys. Rev.* B **62** 1124
[7] Frandsen C, Bahl C R H, Lebech B, Lefmann K, Theil Kuhn L, Keller L, Andersen N H, von Zimmermann M, Johnson E, Klausen S N and Mørup S 2005 *Phys. Rev.* B **72** 214406
[8] Theil Kuhn L, Lefmann K, Bahl C R H, Klausen S N, Lindgård P-A, Frandsen C, Madsen D E and Mørup S 2006 *Phys. Rev.* B **74** 184406
[9] Klausen S N, Lindgård P-A, Lefmann K, Bødker F and Mørup S 2002 *Phys. Status Solidi* a **189** 1039
[10] Bartel L C and Morosin B 1971 *Phys. Rev.* B **3** 1039
[11] Shull C G, Strauser W A and Wollan E O 1951 *Phys. Rev.* **83** 333
[12] Roth W 1958 *Phys. Rev.* **110** 1333
[13] Hutchings M T and Samuelsen E J 1972 *Phys. Rev.* B **6** 3447
[14] Bødker F, Hansen M F, Koch C B, Lefmann K and Mørup S 2000 *Phys. Rev.* B **61** 6826
[15] Low W 1958 *Phys. Rev.* **109** 247
[16] Fernandez V, Vettier C, de Bergevin F, Giles C and Neubeck W 1998 *Phys. Rev.* B **57** 7870

[17] Lefmann K and Rischel C 2001 *Eur. Phys. J.* B **21** 319
[18] Néel L 1961 *C. R. Hebd. Seances Acad. Sci.* **252** 4075
[19] Richardson J T, Yiagas D I, Turk B, Forster K and Twigg M V 1991 *J. Appl. Phys.* **70** 6977
[20] Zhang W S, Brück E, Zhang Z D, Tegus O, Li W F, Si P Z, Geng D Y and Buschow K H J 2005 *Physica* B **358** 332
[21] Makhlouf S A and Parker F T 1997 *Phys. Rev.* B **55** R14717
[22] Bahl C R H, Hansen M F, Pedersen T, Saadi S, Nielsen K H, Lebech B and Mørup S 2006 *J. Phys.: Condens. Matter* **18** 4161
[23] Lindgård P-A, Kowalska A and Laut P 1967 *J. Phys. Chem. Solids* **28** 1357
[24] Bahl C R H, Lefmann K, Jensen T B S, Lindgård P-A, Madsen D E and Mørup S 2006 unpublished
[25] Kondoh H 1960 *J. Phys. Soc. Japan* **15** 1970
[26] Sievers A J and Tinkham M 1963 *Phys. Rev.* **129** 1566
[27] Grimsditch M, McNeil L E and Lockwood D J 1998 *Phys. Rev.* B **58** 14462
[28] Kurosawa K, Miura M and Saito S 1980 *J. Phys. C: Solid State Phys.* **13** 1521
[29] Saito S, Miura M and Kurosawa K 1980 *J. Phys. C: Solid State Phys.* **13** 1513
[30] Pishko V V, Gnatcheko S L, Tsapenko V V, Kodama R H and Makhlouf S 2003 *J. Appl. Phys.* **93** 7382
[31] Lefmann K, Bødker F, Hansen M F, Vázquez H, Christensen N B, Lindgård P-A, Clausen K N and Mørup S 1999 *Eur. Phys. J.* D **9** 491
[32] Bahl C R H, Theil Kuhn L, Lefmann K, Lindgård P-A and Mørup S 2006 *Physica* B at press doi:10.1016/J.Physb.2006.05.234
[33] Bødker F, Hansen M F, Koch C B and Mørup S 2000 *J. Magn. Magn. Mater.* **221** 32
[34] Bahl C R H and Mørup S 2006 *Nanotechnology* **17** 2835
[35] Bahl C R H, Andersen P, Klausen S N and Lefmann K 2004 *Nucl. Instrum. Methods* B **226** 667
[36] Bahl C R H, Lefmann K, Abrahamsen A B, Rønnow H M, Saxild F, Jensen T B S, Udby L, Andersen N H, Christensen N B, Jakobsen H S, Larsen T, Häfliger P S, Streule S and Niedermayer C 2006 *Nucl. Instrum. Methods* B **246** 452
[37] The FullProf software can be found at http://www-llb.cea.fr/fullweb/
[38] Bahl C R H 2006 *PhD Thesis* Technical University of Denmark
[39] Mørup S, Frandsen C, Bødker F, Klausen S N, Lefmann K, Lindgård P-A and Hansen M F 2002 *Hyperfine Interact.* **144/145** 347
[40] Mørup S, Bødker F, Hendriksen P V and Linderoth S 1995 *Phys. Rev.* B **52** 287
[41] Mørup S 1983 *J. Magn. Magn. Mater.* **37** 39
[42] Wivel C and Mørup S 1981 *J. Phys. E: Sci. Instrum.* **14** 605
[43] Shirane G, Shapiro S M and Tranquada J M 2002 *Neutron Scattering with a Triple-Axis Spectrometer* (Cambridge: Cambridge University Press)
[44] Marshall W and Lovesey S W 1971 *Theory of Thermal Neutron Scattering* (Oxford: Oxford University Press)
[45] Srinivasan G and Seehra M S 1984 *Phys. Rev.* B **29** 6295
[46] Mørup S 2003 *J. Magn. Magn. Mater.* **266** 110
[47] Würger A 1998 *Europhys. Lett.* **44** 103